



**HAL**  
open science

## On the generation and propagation of multiple pure tones inside turbofans at transonic regime

J. Thisse, C. Polacsek, S. Léwy, A. Lafitte

► **To cite this version:**

J. Thisse, C. Polacsek, S. Léwy, A. Lafitte. On the generation and propagation of multiple pure tones inside turbofans at transonic regime. AIAA AVIATION - 20th AIAA/CEAS Aeroacoustics Conference, Jun 2014, ATLANTA, United States. hal-01067840

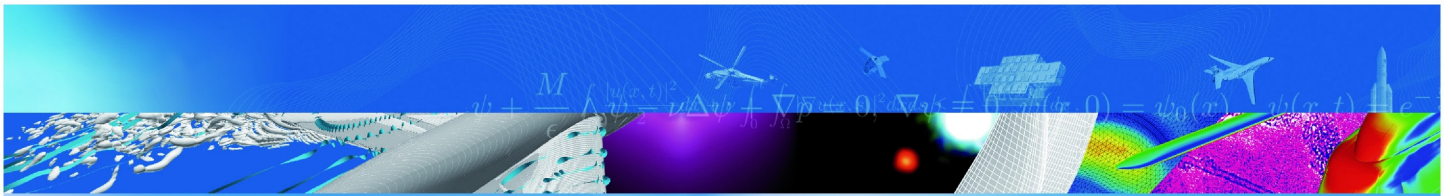
**HAL Id: hal-01067840**

**<https://onera.hal.science/hal-01067840>**

Submitted on 24 Sep 2014

**HAL** is a multi-disciplinary open access archive for the deposit and dissemination of scientific research documents, whether they are published or not. The documents may come from teaching and research institutions in France or abroad, or from public or private research centers.

L'archive ouverte pluridisciplinaire **HAL**, est destinée au dépôt et à la diffusion de documents scientifiques de niveau recherche, publiés ou non, émanant des établissements d'enseignement et de recherche français ou étrangers, des laboratoires publics ou privés.



T I R É À P A R T

**On the generation and  
propagation of multiple pure  
tones inside turbofans at  
transonic regime.**

J. Thisse, C. Polacsek, S. Lewy, A. Lafitte \*

20th AIAA/CEAS Aeroacoustics Conference  
ATLANTA, U.S.A  
16-20 juin 2014

TP 2014-475

**ONERA**

THE FRENCH AEROSPACE LAB

r e t o u r   s u r   i n n o v a t i o n



On the generation and propagation of multiple pure tones inside turbofans at transonic regime.

*Génération et propagation des sons harmoniques de la rotation des soufflantes de  
turboréacteurs aux régimes transsoniques.*

par

J. Thisse, C. Polacsek, S. Lewy, A. Lafitte \*

\* Snecma - Villaroche

**Résumé traduit :**

Tandis qu'en phase d'approche, le bruit rayonné par l'entrée d'air d'un turboréacteur est principalement dû aux interactions rotor-stator, des ondes de choc (ou ondes en N) générées par le rotor en régime transsonique peuvent devenir une source de bruit prédominante durant le décollage et la montée de l'avion. L'étude des ondes en N nécessite de porter une attention particulière à deux processus majeurs : (i) La génération des ondes en N émises par un rotor parfait (dont toutes les aubes sont identiques), ou par un rotor irrégulier (dont les aubes présentent des défauts géométrique); (ii) La propagation des ondes en N à travers la nacelle, qui émettent du bruit dont le spectre contient des fréquences multiples du passage des aubes (rotor parfait), ainsi que des fréquences multiples de la rotation du rotor (rotor irrégulier). Durant les quarante dernières années, plusieurs approches de génération et de propagation des ondes en N ont été étudiées. Cet article se propose de recouper les principales méthodes existantes en les appliquant à deux maquettes de turboréacteur. De plus, une approche prospective de génération des ondes en N basée sur la géométrie des aubes est étudiée grâce à des enregistrements de signaux de pression, croisés aux mesures des angles de calage d'aubes d'un rotor en rotation. Cette nouvelle méthode a pour but de réduire le niveau de pression sonore des fréquences multiples de la rotation en proposant une organisation adéquate des aubes sur le rotor.

---



# On the generation and propagation of multiple pure tones inside turbofans at transonic regime

Johan Thisse\*, Cyril Polacsek†, Serge Léwy‡

*Onera - The French Aerospace Lab*

*F-92322 Châtillon, France*

Anthony Lafitte§

*SNECMA, Acoustics Division - Villaroche, France*

Whereas the sound radiated from the inlet of turbofans is mainly due to rotor-stator interactions in approach flight, the shock waves (or N-waves) emitted by the rotor at transonic rotation speeds can be a dominant noise source during takeoff and climb. The study of N-waves needs to take account of two main processes: (i) The generation of N-waves for a perfect rotor (where all blades are identical) and for a real rotor (considering small geometrical blade dispersion); (ii) The N-wave propagation through the inlet duct producing the blade passing harmonics for a perfect rotor, and the multiple pure tones (harmonics of the rotation frequency) for a real rotor. Several approaches have been investigated for the past forty years. This paper intends to cross-check the main methods by applying them to two modern turbofan demonstrators. Moreover, a prospective way of N-wave generation based on geometrical considerations is investigated thanks to test data related to pressure signal and blade stagger angle measurements during the engine rotation. This prediction overcomes some drawbacks of other methods. Moreover, it appears to be very efficient to build rotor blade orderings that reduce the sound pressure level of the multiple pure tones.

## I. Introduction

The maximum rotational speed of a turbofan is reached during take-off and climb. During these phases the rotor tips are supersonic and spinning shock waves propagate from the fan to the intake, inducing noise radiated towards the fore part of the fuselage and more generally in the upstream far-field. For a perfect fan, the acoustic spectrum only contains harmonics of the Blade Passing Frequency (BPF),  $f_{BPFn} = nBN$ , where  $B$  is the number of blades,  $N$  the rotational speed in Hz, and  $n$  the harmonic order. However, for a real turbofan, small blade geometrical dispersion, e.g., stagger angle variations, produce N-wave amplitude and inter-shock spacing variations which affect their non-linear propagation. These small irregularities lead to spectral components at harmonics of the rotation frequency. So, the acoustic spectrum contains not only BPF harmonics but also Multiple Pure Tones (MPT) where  $f_{MPTm} = mN$ . The non-linearity of the propagation induces two main consequences: (i) The Sound Pressure Level (SPL) decreases as reminded in Section II; (ii) Some acoustic power is transferred from BPF to MPT, as predicted by several methods discussed in Section III. Prediction of the BPF intensity at the end of the ducted propagation is not sufficient. Due to energy redistribution from BPF to MPT during the propagation, some MPT harmonics (which may not be much attenuated by acoustical liners) can be louder than BPF. To predict the spectrum shape has become a main concern for engine manufacturers. Previous studies were focused on MPT 2D non-linear propagation. Morfey & Fisher<sup>1</sup> described the attenuation of a N-wave shock strength during the propagation for a perfect rotor. Then, Hawkings<sup>2</sup> established a temporal method which propagates a N-wave signal with

\*PhD Student, Computational Fluid Dynamics and Aeroacoustics Departement, johan.thisse@onera.fr

†Research Engineer, Computational Fluid Dynamics and Aeroacoustics Departement, cyril.polacsek@onera.fr

‡Research Director, Computational Fluid Dynamics and Aeroacoustics Departement, serge.lewy@onera.fr

§Research Engineer, SNECMA, anthony-b.lafitte@sneema.fr

shock strength irregularities. This temporal method was extended by Uellenberg<sup>3</sup> who included both N-wave phase and amplitude variations. The most sophisticated 2D propagation method is the McAlpine & Fisher spectral approach,<sup>4</sup> improving their temporal approach - that already addressed the problem of N-waves irregularities - by taking into account cut-off modes and acoustic liner absorption. Concerning the MPT generation, two main techniques have been investigated. In the seventies, Pickett<sup>5</sup> proposed a statistical analysis to generate a temporal signal based on the standard deviations of shock strength and of shock spacing. More recently, McAlpine & Fisher used SPL measurements near the fan and random phases to generate the time signal. A third method based on the measurement of the blade stagger angles is proposed in the present paper. The three approaches are tested and compared for two rotor models in Section IV, using time and spectral propagation methods. The first case is a turbofan model which was tested in the framework of the European project FANPAC, and the second is a scale-one new turbofan demonstrator from SNECMA, named MASCOT2. To the authors' knowledge, it is the first time that several methods predicting the generation and propagation of MPT in very different ways are cross-checked.

In complement of these semi-analytic approaches, a few recent numerical studies have been carried out, using Euler and Reynolds-averaged Navier-Stokes (RANS) solvers in 2D and 3D domains. Prasad<sup>6</sup> studied the viscous effects in the N-waves propagation process, and Gliebe *et al.*<sup>7</sup> proposed a method to generate MPT through numerical simulations of a limited number of blade passages. Coupland *et al.*<sup>8</sup> performed a 3D computational fluid dynamics (CFD) simulation of a full rotor coupled with a computational aeroacoustics (CAA) calculation taking into account an acoustical liner. The work presented in this paper only focuses on semi-analytic models, and constitutes the first part of a PhD thesis. The present results will be compared in a second step with numerical simulations performed using the ONERA *elsA* code (solving Euler equations).

## II. N-wave propagation

The N-wave propagation comes from non-linear effects due to sound velocity variations. The sound velocity is given by:

$$c = c_0 \left( 1 + \frac{\gamma - 1}{2\gamma} \frac{\Delta p}{p_0} \right), \quad (1)$$

with  $c_0$  the sound velocity in the undisturbed fluid at the atmospheric pressure  $p_0$ ,  $\gamma$  the adiabatic ratio, and  $\Delta p$  the pressure jump. For a transonic turbofan, the relative Mach number  $M_{rel}$  at the blade tips is greater than one, and shock waves are generated. The pattern of  $B$  N-waves corresponding to the  $B$  rotor blades propagating upstream toward the intake is illustrated in Fig. 1. For a perfect rotor, each N-wave has the same shock amplitude  $\overline{\Delta p}$ , wavelength  $\overline{\Lambda}$  and shock spacing  $\overline{\lambda}$  (Fig. 1(b)), depending on the geometrical configuration and the rotational fan speed:

$$\overline{\Lambda} = \overline{\lambda} = \frac{\pi D}{B} \sin(\alpha + \beta - \pi/2), \quad (2)$$

where  $D$  is the rotor diameter,  $\alpha$  is the angle between the relative Mach number  $M_{rel}$  and the axial Mach number  $M_x$  such as  $\cos \alpha = M_x/M_{rel}$ , and  $\beta$  is the Mach angle such as  $\sin \beta = 1/M_{rel}$ . For a real fan, the amplitudes and shock wave spacings are different from one N-wave to another one, and  $\overline{\lambda}$  and  $\overline{\Delta p}$  then are the N-wave mean values.

The N-waves are evolving during inlet propagation. For a regular rotor, the shock spacings ( $\overline{\lambda}$ ) remain constant and the pressure jumps decrease. A first theory was developed by Morfey & Fisher<sup>1</sup> to determine the evolution of the shock wave amplitude during propagation, valid for regular N-waves (ideal rotor). The pressure jump writes:

$$\overline{\Delta p}(t) = \frac{\overline{\Delta p}(0)}{1 + \frac{\gamma+1}{2\gamma} \frac{\overline{\Delta p}(0)}{p_0} \frac{c_0 t}{\overline{\lambda}}} \quad (3)$$

If irregularities on  $\Delta p$  or  $\lambda$  are present in the initial signal, not only the pressure jumps but also the shock intervals are modified. Hawkings<sup>2</sup> proposed a method based on variations of the N-wave slopes to predict the propagation of a sawtooth with amplitude irregularities. Uellenberg<sup>3</sup> extended this work and also took into account variations of shock spacings ( $\lambda$ ). At last, McAlpine & Fisher<sup>4</sup> developed a numerical solution to propagate a pressure signal in the frequency domain. The wavenumber Fourier series,  $C_m$ , of the pressure is defined as:

$$P(X, T) = \sum_{m=-\infty}^{\infty} C_m(T) e^{jmX},$$

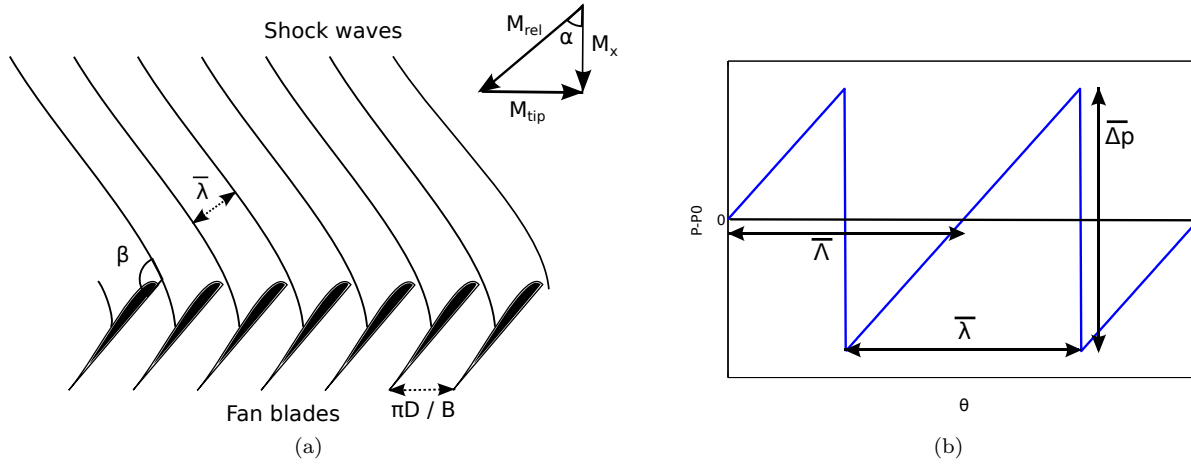


Figure 1. (a) Shock wave generated by an even rotor; (b) Regular N-wave diagram

with the adimensionalized time  $T$ , distance  $X$ , and pressure  $P$  respectively equal to:

$$T = \frac{c_0 t}{\lambda}, X = \frac{2\pi x}{B\lambda}, P = \left( \frac{\gamma + 1}{2\gamma} \right) \frac{\Delta p}{p_0}.$$

A mode  $m$  correspond to the frequency  $f_{MPTm} = mn$ . Fourier coefficients  $C_m(T)$  are solutions of the Burgers equation with two dissipative terms:

$$\frac{dC_m}{dT} = -\frac{jm\pi}{B} \left( \sum_{l=1}^{m-1} C_{m-l} \tilde{C}_l + 2 \sum_{l=m+1}^N C_l \tilde{C}_{l-m} \right) - \varepsilon \frac{m^2}{B^2} C_m - \sigma(m) C_m. \quad (4)$$

where  $C_m$  is the  $m$ th spectral component,  $\tilde{C}_m$  its complex conjugate. The first term in parentheses on the right hand side in Eq. (4) expresses the energy redistribution between each harmonic during the propagation, the second term is the numerical dissipation due to the truncation of the solved spectrum (up to the harmonic order  $N = 10B$ ), and the last term takes account of cut-off modes and of acoustical liner absorption. These two properties in the last term cannot be introduced in a time domain method (also implemented by Morfey & Fisher)<sup>4</sup> which explains the interest to work in the frequency domain.

### III. Predictions of MPT generation for a real rotor

For a regular rotor, the  $n$ th BPF SPL and the overall sound pressure level (OASPL) are linked to the shock wave amplitude according to Eq.(5) and Eq.(6):

$$SPL(BPF_n) = 20 \log \left( \frac{p_n^{rms}}{p_{ref}} \right) \quad (5)$$

$$OASPL = 20 \log \left( \frac{p^{rms}}{p_{ref}} \right) \quad (6)$$

where  $p_{ref} = 2.10^{-5}$ Pa, the root mean square pressure (rms) of the  $n$ th component is  $p_n^{rms} = \frac{\overline{\Delta p}}{n\sqrt{2\pi}}$ , and overall rms pressure  $p^{rms} = \frac{\overline{\Delta p}}{2\sqrt{3}}$  for a regular N-wave. The MPT generation is more complex and several approaches can be considered.

#### A. Statistical method

The first MPT generation model due to Pickett<sup>5</sup> and is based on statistical analysis. Values of standard deviations with respect to shock amplitude and shock spacing were deduce from fan rig measurements. The method consists in a random selection of  $B$  shock amplitudes ( $\Delta p$ ) and spacings ( $\lambda$ ) of standard deviations



$\sigma_A$  and  $\sigma_\lambda$ , respectively. The pressure time signal linked to the shock wave train induced by a real rotor (with irregularities) writes:

$$p(t) - p_0 = \sum_{i=0}^{B-1} A_i \times \left[ t - (i + \epsilon_i) \frac{\bar{\lambda}}{c_0} \right], \quad (7)$$

with  $\langle A_i \rangle = \frac{c_0 \overline{\Delta p}}{\bar{\lambda}}$  and  $\langle \epsilon_i \rangle = 0$ . Its power spectral density  $S(m)$  is given by:

$$S(m) = 2B^2 |F_0(m)|^2 \left\{ \exp \left[ - (2\pi m \sigma_\lambda / B)^2 \right] \delta_{m,nB} + \frac{(1 + \sigma_A^2) - \exp \left[ - (2\pi m \sigma_\lambda / B)^2 \right]}{B} \right\}, \quad (8)$$

where  $C_0(m)$  is the Fourier transform of the pressure jump attached to one blade of the perfect rotor ( $m = 1$  is the fundamental MPT,  $m = B$  the fundamental BPF), and  $\delta_{m,nB}$  is the Kronecker symbol. The attenuation  $\Delta_{SPL}$  between a BPF harmonic  $n$  from a regular rotor ( $S_B(nB) = 2B^2 |F_0(nB)|^2$ ) and from an uneven rotor ( $S(m = nB)$ ) is:

$$\Delta_{SPL}(nB) = \frac{B-1}{B} \exp \left[ - (2\pi n \sigma_\lambda)^2 \right] + \frac{1}{B} (1 + \sigma_A^2) \quad (9)$$

Figure 2 depicts an example of the method. A random pressure signature is shown in Figure 2(a), and the mean spectrum of 100 random signals is compared to the analytical spectrum of Eq. (8) on the right hand side. Kurosaka<sup>9</sup> and Stratford & Newby<sup>10</sup> pointed out that differences between shock amplitudes (where  $\sigma_A \leq 0.3$  in representative turbofan conditions) are less significant than those between shock spacings (as is shown in the term  $1 + \sigma_A^2 < 1.1$  for  $\sigma_A \leq 0.3$  in Eqs. (8 and 9)). Lewy & Polacsek<sup>11</sup> applied this statistical approach to the FANPAC turbofan model and provided suited values of the two standard deviation using Eq. (9) by matching the SPL decrease measured on BPF.

This statistical method based on standard deviation is efficient and quite simple but requires to adjust the value of  $\sigma_\lambda$ .

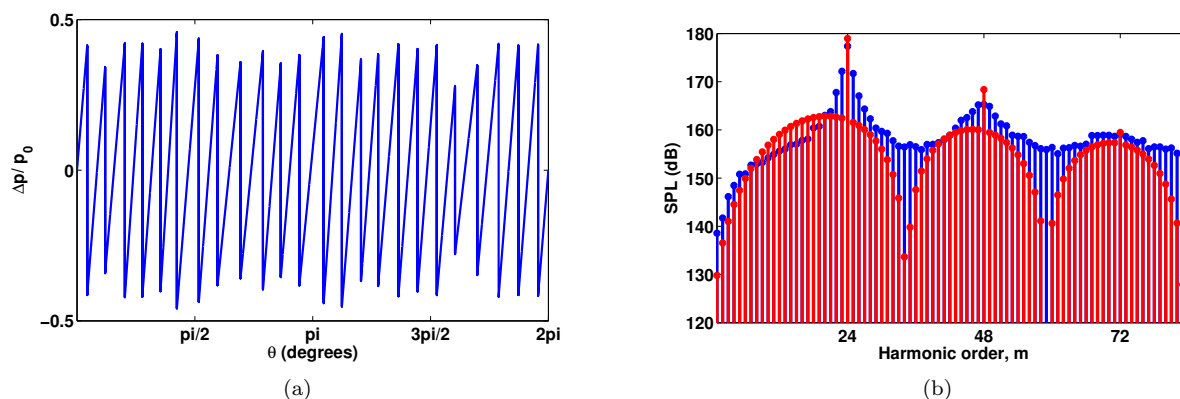


Figure 2. Example of MPT generation for a 24-bladed rotor: (a) Time signal; (b) Mean spectrum of 100 random selections (blue) and statistical spectrum from Eq. (8) (red).

## B. Method based on measurements near the rotor

In another approach developed by McAlpine & Fisher,<sup>4</sup> the shock-wave signal is generated using the spectra measured near the fan combined with a distribution of random phases (because the time signature or the complex Fourier transform usually are not recorded). Two hypotheses are done to reconstruct the signal (used in Section IV.B and Section IV.C):

- All pressure jump amplitudes of the N-wave signal are equal (and can be estimated from measurements by Eq. (5) or Eq. (6));
- The slopes of the N-waves are constant.

The shock spacings thus directly depend on the difference of mid-pressure (such as  $p_{m1}$ ) between shocks  $i$  and  $i + 1$ , as is shown in Fig. 3(a). Assuming that the SPL of  $BPF_1$  and of the MPT are known (e.g., from measurements, in Fig. 3(c) in red), the shock amplitude is calculated. The irregularities in signal phases come from the variations of N-wave shock mid-points ( $p_{m1}$  in Fig. 3(a)). These variations are set thanks to SPL of  $B$  MPT (from  $m = B$  to  $m = 2B - 1$  in Fig. 3(c)). Figure 3 highlights the signal reconstruction using the McAlpine & Fisher method with a pressure signal (3(a)), the associated spectrum (3(b)), and the mean spectrum of 10 pseudo-randomized signals (3(c)).

This method was successfully applied to a Fokker 100 model, but the main limitation is the requirements of the pressure spectral component near the fan for every cases.

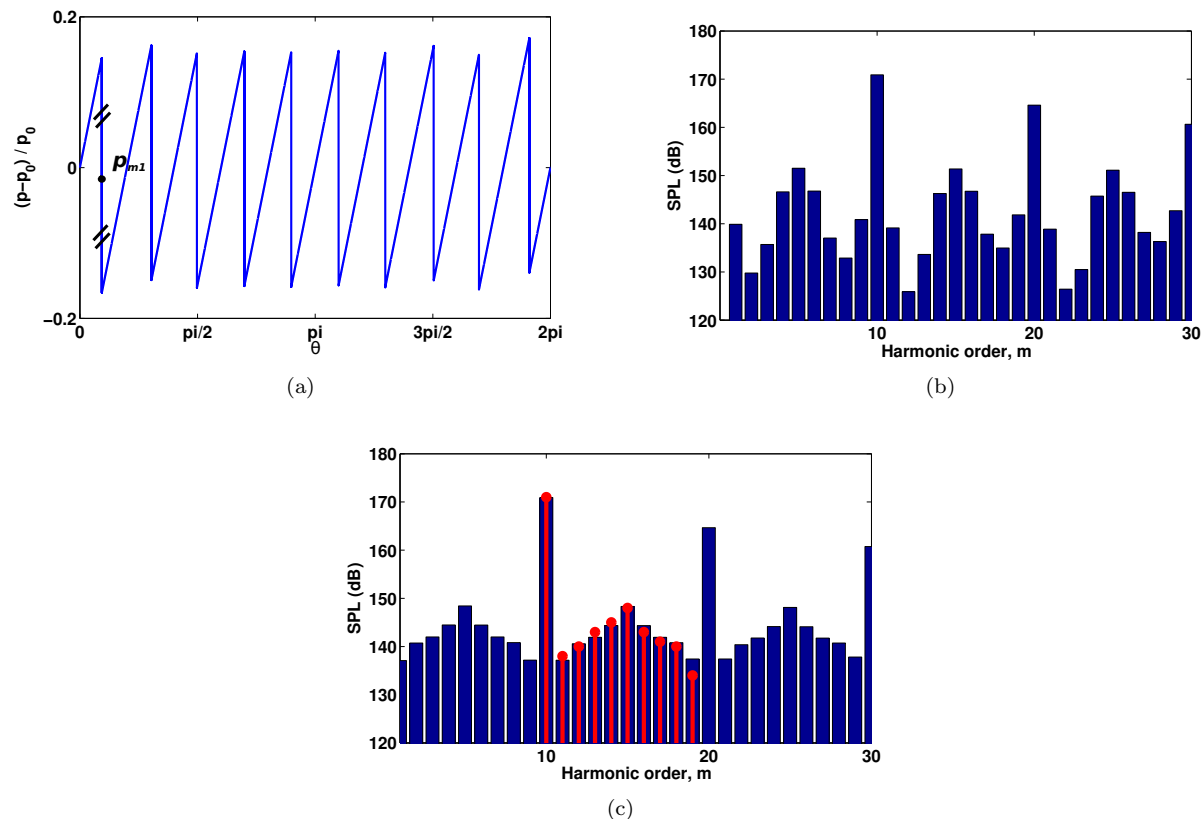


Figure 3. McAlpine & Fisher method: (a) Pressure signal of a 10-bladed rotor; (b) Frequency spectrum; (c) Mean spectrum of 10 generated pressure signals (blue) compared to the measured SPL spectrum (red)

### C. Novel method based on measurements of blade stagger angles

In order to overcome the previous limitations, ONERA developed a new approach which only requires the real blade geometries in only one configuration. During the full-scale MASCOT2 engine model tests (see Section IV below), not only pressure signatures were recorded, but also the individual blade stagger angle at several rotational speeds. Thanks to several numerical simulations, Gliebe *et al.*<sup>7</sup> showed that blade stagger angle (and camber) variations mainly affect the N-wave signals. Moreover, a variation of the  $i$ -blade stagger angle not only modifies the shock spacing  $\lambda_i$  between the waves  $i$  and  $i + 1$  (cf. Fig. 4), but also of the two adjacent shock spacing  $\lambda_{i+1}$  and  $\lambda_{i-1}$ . In this sub-section, a prospective approach of N-wave generation based on basic geometrical considerations is investigated. To study the rotor acoustic spectrum shape, three configurations corresponding to three different blades orderings on the rotor were tested (Confs. 1, 2, and 3). Knowing the shock spacing and the temporal pressure signature near the fan of one configuration (e.g., Conf. 1), the temporal signals are predicted for other configurations (e.g., Confs. 2 and 3). Assuming that only the stagger angle variations of blades  $i$ ,  $i + 1$ ,  $i - 1$  induce a variation of the shock spacing  $\lambda_i$ , an experimental relation is established between stagger angle variations ( $i$ ,  $i + 1$ ,  $i - 1$ ) and  $\lambda_i$ .

The pressure signal generation consists of three steps. (i) The blade stagger angles of the reference configuration (Conf. 1) are reorganized according to the blade arrangements of the other configurations (Confs. 2 and 3). (ii) The  $\lambda_i$  are estimated between each couple of the reference blades according to the relation between stagger angles and shock spacing variations. The pressure jumps are assumed to be the same regardless of the configuration, so  $\Delta p$  is set from reference configuration (Conf. 1). (iii) The pressure signature is generated using  $\lambda_i$  and  $\Delta p$  following the McAlpine & Fisher approach. Perturbations are introduced in the  $\lambda_i$  because of stagger angle variations during the rotor rotation. The resulting buzz-saw noise spectrum is an averaged spectrum from 10 pressure signatures.

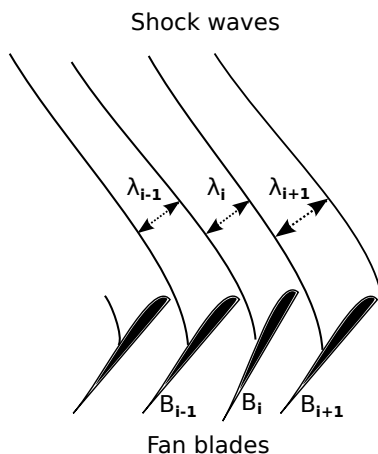


Figure 4. Uneven rotor shock waves

1. *Experimental relation between blade stagger angles and time signal (in the reference case)*

The blade stagger angle measurement provides the blade stagger angles during the engine rotation (see Section IV.C). Because of small variations of the fan rotational speed and unsteady blade twist, the blade stagger angles vary during the engine rotation. So, stagger angle mean values ( $Stg_i$ ), and a standard deviation ( $\sigma_{Stg}$ ) are deduced from the measurements. As is highlighted in Figure 11 (Section IV.C),  $Stg_i$  is the time averaged measured stagger angle of blade  $i$  and  $\sigma_{Stg}$  is the standard deviation of the stagger angles. These values depend on the rotational speed. An experimental relation is established between stagger angle and shock spacing of each blade in the reference configuration (Conf.1). The method consists in four steps (see the flowchart in Fig. 5:

- (i) For one rotational speed,  $\bar{\lambda}$  is determined using Eq. (2). The stagger angle variations  $\Delta Stg_i$  are determined from the measurements such as  $\Delta Stg_i = Stg_i - \frac{1}{B} \sum_{i=1}^B Stg_i$ . Coefficients  $\mu_0, \mu_{+1}, \mu_{-1}$  are arbitrarily chosen, and the shock spacings  $\lambda_i^*$  are estimated using Eq. (10):

$$\lambda_i^* = \bar{\lambda} (1 - \mu_0 \times \Delta Stg_i + \mu_{-1} \times \Delta Stg_{i-1} + \mu_{+1} \times \Delta Stg_{i+1}) \quad (10)$$

- (ii) The pressure time signature  $p(t)$  is measured by Kulite transducers near the fan which gives the shock spacing  $\lambda_i$  of the N-wave  $i$  corresponding to the blade  $i$ . An efficient process has been set up to relate the stagger angles  $Stg_i$  to the pressure time signature  $p_i(t)$ . Indeed, because sensors recording blade stagger angles are not at the same axial position than Kulite transducers, a second minimization process is applied. This result gives the blade order  $k$  corresponding to the first shock measured by the Kulite transducers upstream of the stagger angle sensors. The process minimizes the error between measured shock spacings and shock spacings generated from different blade order  $k$ :  $\xi(k) = \sum_{i=1}^B |\lambda_i - \lambda_i^*(k)|^2$ , where  $k$  is shifted from 1 to  $B$ . Figure 6 illustrates an application of this process (on the MASCOT2 rotor configuration described in section IV.B), where the blade order generating the first shock recorded is  $k = 12$  in this case.
- (iii) The final values of  $\mu_0, \mu_{+1}$ , and  $\mu_{-1}$  are computed thanks to a minimization algorithm between  $\lambda_i^*$  and  $\lambda_i$ .

- (iv) The shock pressure  $\Delta p$  is estimated from the Kulite pressure transducer measurements and the McAlpine & Fisher N-waves generation (described in Section III.B).

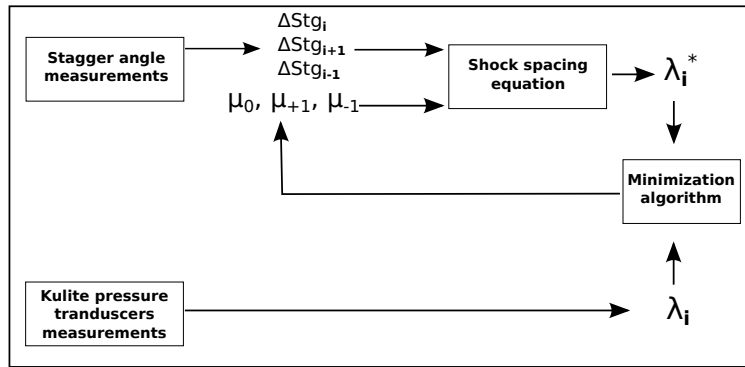


Figure 5. Flowchart of the N-wave generation process

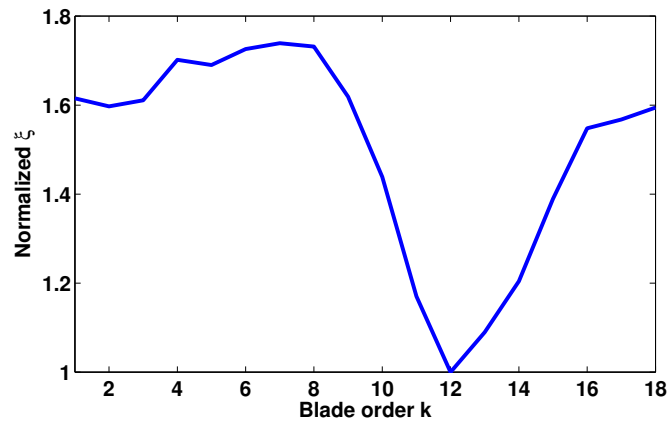


Figure 6. Determination of blade order  $k$  (related to N-wave signature)

This method is duplicated at each rotational speed, and the coefficients used in the N-wave generation are the mean values from all rotations speeds for each index  $i$ .

## 2. Application of the method to another configuration with a different blade ordering

Using the coefficients  $\mu_0, \mu_{+1}$ , and  $\mu_{-1}$  (obtained from the reference configuration), new pressure signals are now predicted in another configuration (Conf. 2 or 3), that is to say, for another organization of blades on the rotor. Therefore the shock spacings  $\lambda_i^*$  are determined from the new blades ordering generating a new set of values  $\Delta Stg_i$ , and using the reference values of coefficients  $\mu_0, \mu_{+1}$ , and  $\mu_{-1}$ . Due to unsteady blade twist, variations of  $\Delta Stg_i$  are introduced using  $\sigma_{Stg}$ . For one predicted pressure signal, the  $Stg_i$  (and thus  $\Delta Stg_i$ ) in Eq. (10) are pseudo-randomized using a Gaussian distribution of mean  $Stg_i$ , and of standard deviation  $\sigma_{Stg}$  assumed to be the same for all configurations. Hence, for one blade order, with the aim of taking account of unsteady blade twist, several  $\lambda_i^*$  are obtained leading to several time pressure signals. The mean shock pressure depending only on the rotational speed, the  $\overline{\Delta p}$  from the reference configuration are used. The resulting spectrum is a mean of 10 Fourier transforms of pseudo-randomized signals.

## IV. Applications to turbofan models

The different approaches for the MPT generation, and temporal and spectral propagation methods are compared in this section. First in order to check the equivalence of time and frequency domain predictions,

a virtual 7-blade time signature with  $\Delta p = 50$  kPa is propagated according to the Uellenberg (temporal) and McAlpine & Fisher (spectral) methods. The third N-wave has a pressure variation  $\Delta p' = 1.5\Delta p$ . Figure 7(a) presents the time signature evolution, and the sound pressure level of the first three BPF tones are shown in Fig. 7(b). The two methods agree quite well. The time signatures slightly differ because the McAlpine & Fisher method solves the MPT only up to engine order  $10 B$ .

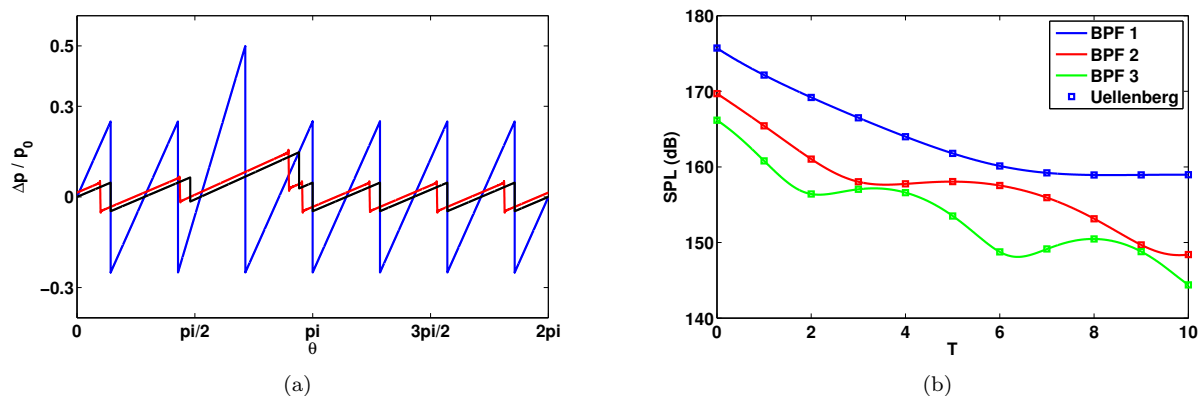


Figure 7. Comparison of Uellenberg and McAlpine & Fisher propagation methods. (a) Time signature at  $T=0$  (blue), propagated signal using McAlpine & Fisher method (red) and Uellenberg method (black). (b) Variation of SPL for  $BPF_1$ ,  $BPF_2$ ,  $BPF_3$  using McAlpine method (solid lines) and Uellenberg method (squares).

### A. FANPAC turbofan model

A turbofan model has been tested in the European FANPAC project. Its main characteristics are given in Table 1. The reduced time  $T$  introduced in Section II can be related to the traveled axial distance,  $x$ , as:

$$T = c_0 t / \lambda = (x/D) K, \quad (11)$$

with  $T = T_f$  at the end of the inlet, for  $x = 0.5$  m, and  $K$  depending on the Mach numbers:

$$K = \frac{B}{\pi} \frac{M_{rel}^4}{\sqrt{M_{rel}^2 - 1}} \left( M_x \sqrt{M_{rel}^2 - 1} - M_{tip} \right)^{-2}$$

Rotor diameter $D$ (m)	Number of blades $B$	Rotational speed $N$ (rpm)
0.870	24	8083
Blade tip Mach number $M_{tip}$	$M_x$	$M_{rel}$
1.085	0.29	1.12
$\Delta P(0)$ (Pa)	$F_{MPT}$ (Hz)	$F_{BPF}$ (Hz)
95200	135	3240

Table 1. Main characteristics of the FANPAC model.

The FANPAC configuration gives  $\bar{\lambda} = 0.085$  m and  $T_f = 15.5$  which corresponds to a dimensionalized time  $t_f = 3.9 \cdot 10^{-3}$  s. The McAlpine & Fisher propagation method is compared to the two temporal methods of Hawkins and Uellenberg for the ideal FANPAC rotor. These two methods for a regular fan provide the same results, as is highlighted in Fig. 8. The difference in the last BPF harmonic ( $n = 10$ ) are due to the spectrum truncation. The regular case is compared with FANPAC measurements in Fig. 8(a), (squares). The SPL at  $BPF_1$  was measured at several distances in the inlet (i.e., at several propagation times  $T$ ). The differences in  $BPF_1$  between SPL predicted for an ideal rotor and measured forward of the real rotor (roughly equal to 3 dB at the end of the duct) are due to the acoustic power redistribution from the BPF to the MPT.

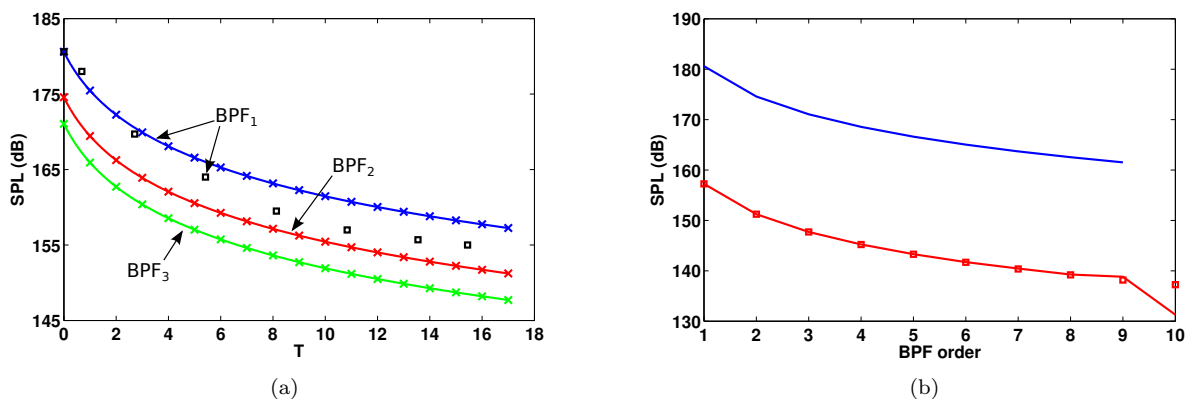


Figure 8. (a) SPL decrease of the first three BPF, frequency (solid lines) and temporal (crosses) methods compared to FANPAC measurements at  $BPF_1$  (squares). (b) BPF harmonics at  $T = 0$  (in blue) and at  $T_f$  (in red), according to McAlpine & Fisher (solid line) and temporal (squares) methods

Pickett statistical method is applied to generate MPT. As  $\sigma_A$  is of little importance against  $\sigma_\lambda$ , a modern turbofan typical value is chosen ( $\sigma_A = 0.1$ ). As mentioned in Section III.A, the standard deviation of shock spacing is estimated using Eq. (9) and  $\Delta_{SPL}(B)$ . The SPL difference at  $BPF_1$  between regular rotor and FANPAC measurements at  $T_f$  (Fig. 8(a)) leads to  $\Delta_{SPL}(B) \simeq 3$  dB, thus the standard deviation of shock spacings at the end of propagation is roughly  $\sigma_\lambda = 0.14$ . As standard deviations evolve during propagation, the initial  $\sigma_\lambda$  leading to 0.14 at  $T_f$  is found by iterations. Figure 9 highlights the capability of the Pickett's method. In Figure 9(a), the  $\sigma_\lambda$  evolution matching  $\sigma_\lambda = 0.14$  at  $T_f$  is displayed. On the right hand side, the decrease of SPL at  $BPF_1$  during propagation is compared to the regular rotor and to FANPAC measurements. The agreement with experiment is better showing that such a statistical method can easily predict the SPL decrease including energy redistribution from BPF to MPT during the propagation.

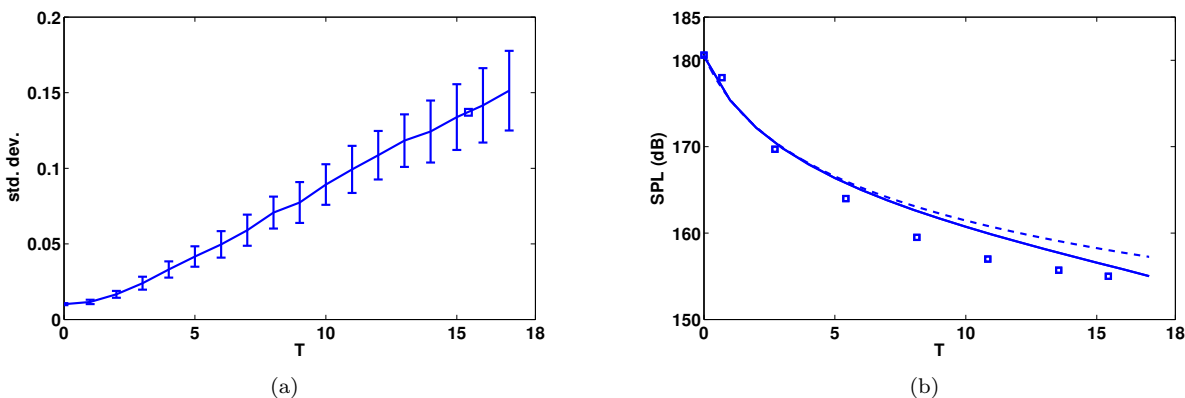


Figure 9. (a) Evolution of standard deviation  $\sigma_\lambda$  during the propagation, with the FANPAC target value (square); (b) SPL decrease at  $BPF_1$  for the average of 10 propagated irregular signals (solid line) compared with the ideal case (dashed line) and FANPAC measurements (squares).

## B. MASCOT2 turbofan model

The second turbofan model is a SNECMA turbofan scale-one model called MASCOT2. The MASCOT2 characteristics are listed in Table 2. Three configurations corresponding to three different blade ordering on the rotor are selected to analyze the spectrum variations according to the blade arrangement. The values of  $\bar{\lambda}$ ,  $T_f$  and  $t_f$  are similar in the three configurations ( $\bar{\lambda} = 0.148\text{m}$ ,  $T_f = 31.8$ ,  $t_f = 0.014\text{s}$ ).

Thanks to the pressure measurements near the fan, the temporal signatures can be reconstructed using the McAlpine & Fisher method, and propagated through the inlet using their spectral method.<sup>4</sup> The

Rotor diameter $D$ (m)	Number of blades $B$	$M_{tip}$	$\Delta p$ (Pa)
1.78	18	1.03	20000

**Table 2.** Main characteristics of the MASCOT2 tests

MASCOT2 tests provided the SPL spectra at two axial positions: near the fan (plane  $p1$ ) and near the intake section (plane  $p2$ ), recorded by five wall-mounted Kulite pressure transducers (three in  $p1$  and two in  $p2$ ). The distance between the two planes is 1.42 m. The temporal signals of the Kulite transducers were recorded during 30 s, up to a frequency of 50 kHz. A fast Fourier transform using the Welch method with a Hanning window is applied. At last, an average spectrum is computed in each plane. Although the measurements provide the spectral amplitudes and phases, in order to apply the McAlpine & Fisher MPT generation method, only the spectra amplitudes are used, and the phases are pseudo-randomized. In the same way as McAlpine *et al.*,<sup>12</sup> the spectral component  $C_m$  have been propagated and agree quite well with the measurements. SPL spectra from the McAlpine & Fisher approach are compared to MASCOT2 measurements in Fig. 10. Spectra are in a good agreement close to the fan. Near the inlet, the spectrum slopes are well predicted, as well as the maxima of the first MPT and of the  $BPF_1$  which mainly contribute to OASPL.

### C. ONERA novel approach applied to MASCOT2 model configuration

The novel approach based on measurements of stagger angles (Section III.C) is applied to MASCOT2. The individual blade stagger angles are measured by a couple of capacitive sensors located in the casing at the tip of the blades, and 10 pressure signatures are generated. The reference configuration used to determine which the coefficients  $\mu_0, \mu_{+1}$ , and  $\mu_{-1}$  is Conf. 1. Then, the method is applied to Confs. 1, 2, and 3 to build the pressure signatures and to propagate them using the spectral method.

The coefficients are computed at five rotational speeds. The shock amplitudes are measured at each rotational speed by Kulite pressure transducers. Figure 11 shows the mean shock amplitude in the range of studied rotational speeds obtained by time signals and calculated from the SPL (cf. Eq. (5)) for Confs. 1 and 3. The good agreement between the two configurations validates the assumption that the shock pressures do not depend on the order of the blades. The blade stagger angles are then measured, and the  $\lambda_i^*$  are calculated from arbitrary values of coefficients  $\mu_0, \mu_{+1}$  and  $\mu_{-1}$ . Modifying the coefficients, the algorithm minimizes the difference between the estimated  $\lambda_i^*$  shock spacings, and the measured  $\lambda_i$ . This process is applied for the five rotational speeds, and mean values of the coefficients are calculated. The blade stagger angles are ordered according to the configuration and the final  $\lambda_i^*$  are calculated using the above mean values of  $\mu_0, \mu_{+1}$  and  $\mu_{-1}$ . Figure 12 compares the blade stagger angles determined from the rearrangement of Conf. 1 to Confs. 2 and 3. The predicted stagger angles are close to the measurements. Knowing the  $\lambda_i^*$  and the shocks pressure  $\Delta p$ , the time signals are built. Due to variations of the fan rotational speed and unsteady blades twist, as described in Section III.C, several signals are built from the pseudo-randomization of the blade stagger angles and thus of  $\lambda_i^*$ . Each signal is then propagated by the spectral method and leads to a propagated spectrum (average from 10 pseudo-randomized signals). Figure 13 presents the rebuilt spectra near the fan obtained by the present approach, and the spectra propagated using the spectral method. In all the configurations, the pressure signals are predicted using the stagger angles of Conf. 1 (reorganized for Confs. 2 and 3).

Figure 13 shows that the predicted spectrum shape and the level of BPF agree quite well with the measurements before and after the propagation. Not only the reference configuration (Fig. 13, top) is correctly predicted, but also the two other configurations (Fig. 13, middle and bottom). Using stagger blade angle measurements of a reference configuration, this prospective approach allows us to predict the spectral shapes of other configurations. This method could be very interesting to reduce the SPL because Figs. 10 and 13 show that the MPT strongly depend on the blade arrangement.

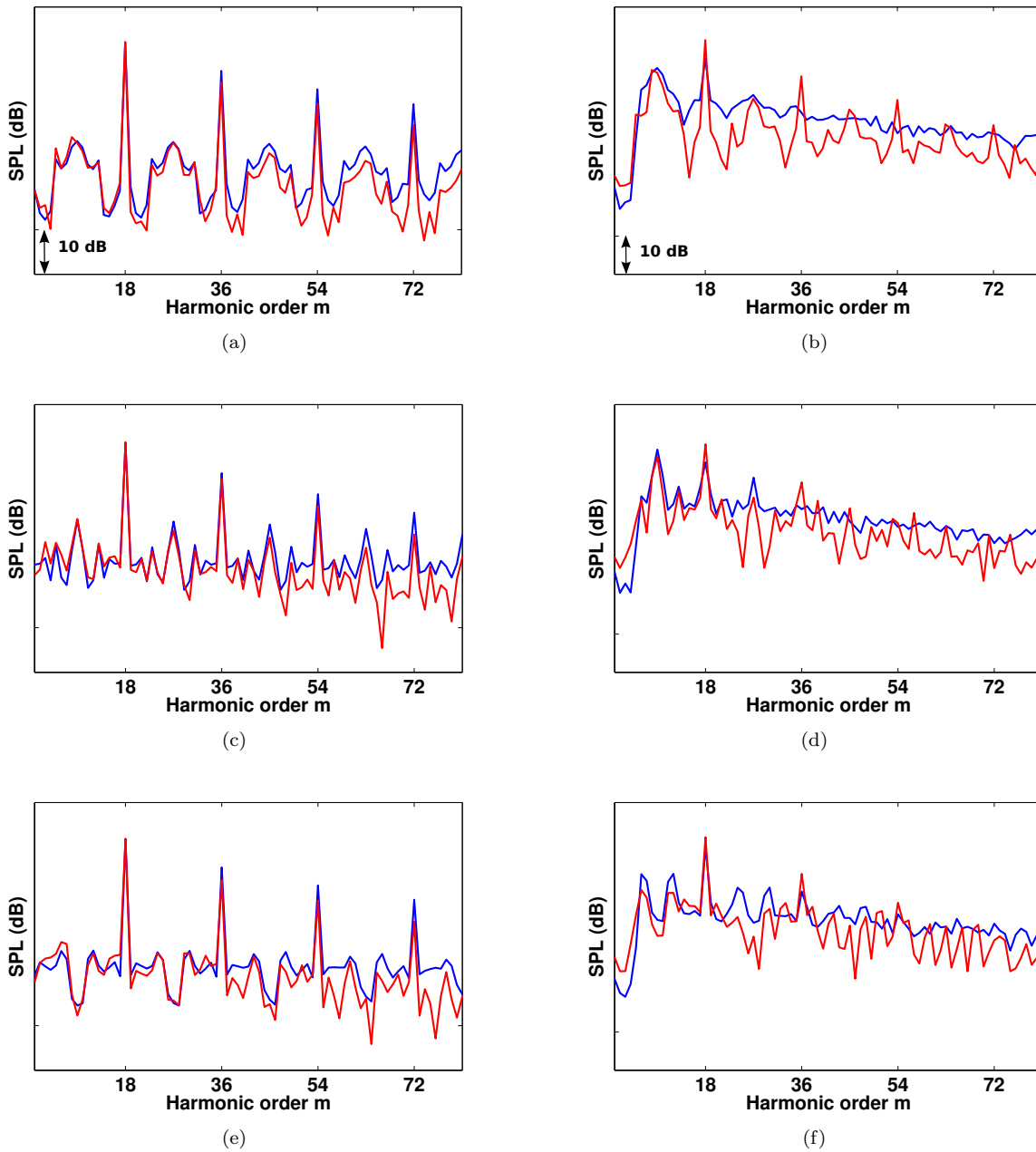


Figure 10. Comparison between measured spectra (red) near the fan (left) and after propagation (right), and spectra deduced from the McAlpine & Fisher N-waves generation method (blue) for the three configurations (Conf. 1 top, Conf. 2 middle, Conf. 3 bottom).



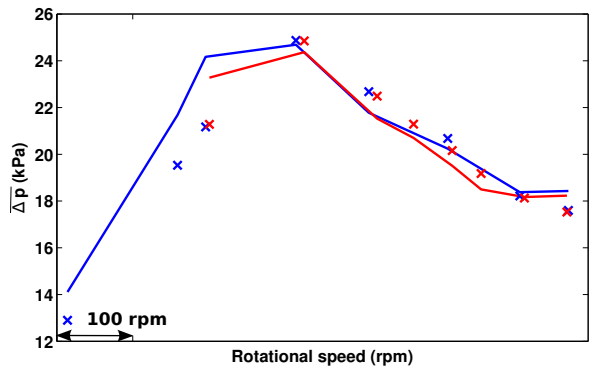


Figure 11. Effect of rotational speed on shock pressures for two configurations. Shock pressures measured (straight lines) and obtained from the OASPL (crosses), for Conf. 1 (in blue), and Conf. 3 (in red).

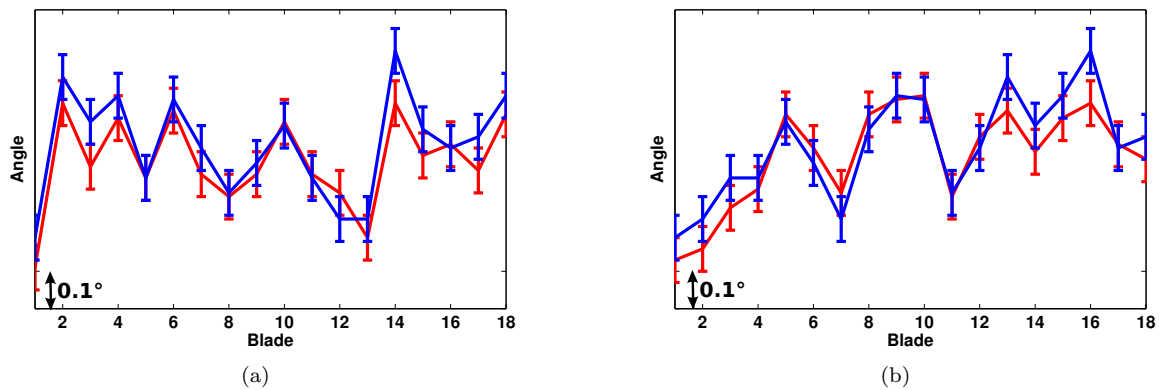


Figure 12. Comparison between measured stagger angles of Confs. 2 and 3 (red) and stagger angles deduced from Conf. 1 reorganized according to the blades orderings (blue) in Confs. 2 (a) and 3 (b).

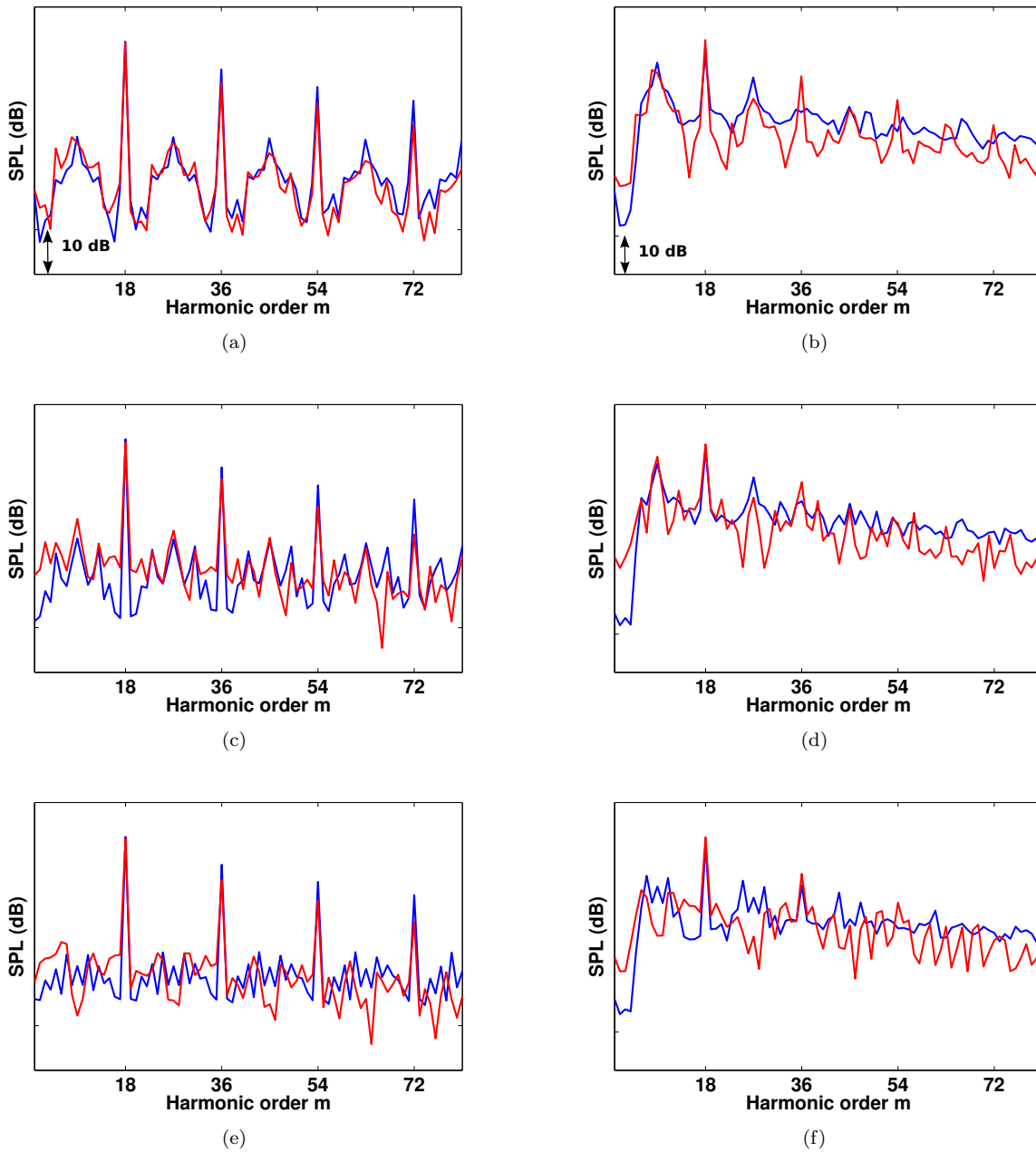


Figure 13. Comparison between measured spectra (red) near the fan (left) and after propagation (right), and spectra deduced from the stagger angles (blue) for the three configurations (Conf. 1 top, Conf. 2 middle, Conf. 3 bottom).

## V. Conclusions and future work

Two key aspects must be considered to describe the shock-wave propagation in the inlet of a transonic turbofan. The first issue is the N-wave propagation, the second is the MPT generation. In this study, the most advanced analytical methods have been compared in the time and frequency domains for two representative turbofan configurations. The reliability of each method has been discussed through a comprehensive analysis and validated using experimental data. More particularly, the MPT generation has been studied through selected approaches. A statistical MPT generation method has been successfully implemented and tested on the FANPAC turbofan model. The McAlpine & Fisher method has been investigated and tested on a MASCOT2 engine model from SNECMA. Predicted spectra and test data are in good agreement. However, the MPT generation process of these approaches requires specific measurements near the fan. Pickett method does not allow us to predict the spectrum shape depending on blade arrangement, and McAlpine & Fisher MPT generation needs to know an initial spectrum.

An original approach of MPT generation based on real blade stagger angles has been proposed and applied to the MASCOT2 engine model. The acoustic spectra depend on the order of the rotor blade, and it is decisive for engine manufacturers to predict in a simple way the spectrum shapes near the fan and at the intake. This new method answers that question since it only requires measurements in one rotor configuration. Acoustic spectra can be predicted for other non-tested blade configurations. An optimal order of the blades can be selected to minimize the radiated sound pressure level, taking into account the cut-on modes and the acoustic liner absorption.

Present work is focused on analytical methods and is included in a PhD thesis. The second part of the thesis will deal with numerical simulations already implemented. Starting from the present results, N-waves will be injected in the ONERA CFD code *elsA*. MPT generation and propagation will be investigated through several computations, and the present theory will be used as reference case for comparisons between analytical and numerical solutions. However, CPU time may be prohibitive for parametric studies, and analytical and numerical calculations will remain complementary.

## References

- <sup>1</sup>Morfey, C. L. and Fisher, M. J., "Shock-wave radiation from a supersonic ducted rotor," *The Aeronautical Journal of the Royal Aeronautical Society*, Vol. 74, No. 715, 1970, pp. 579–585.
- <sup>2</sup>Hawkings, D., "Multiple tone generation by transonic compressors," *J. Sound Vib.*, Vol. 17, No. 2, 1971, pp. 241–250.
- <sup>3</sup>Uellenberg, S., "Buzzsaw noise predictions for modern turbofans," *10th AIAA/CEAS Aeroacoustics Conference, Manchester, UK, AIAA Paper 2004-3000*, 2004.
- <sup>4</sup>McAlpine, A. and Fisher, M. J., "On the prediction of "buzz-saw" noise in aero-engine inlet ducts," *J. Sound Vib.*, Vol. 248, No. 1, 2001, pp. 123–149.
- <sup>5</sup>Pickett, G., "Prediction on the spectral content of combination tone noise," *J. Aircraft*, Vol. 9, No. 9, 1972, pp. 658–663.
- <sup>6</sup>Prasad, A., "Evolution of upstream propagation shock waves from a transonic compressor rotor," *ASME J. Turbomach.*, Vol. 125, 2003, pp. 133–140.
- <sup>7</sup>Gliebe, P., Mani, R., Shin, H., Mitchell, B., Ashford, G., Salamah, S., and Connel, S., "Aeroacoustics prediction codes," Tech. rep., NASA, 2000, Contractor Report CR-2000-210244.
- <sup>8</sup>Couplan, J., Wilson, A., Pollard, N., Uellenberg, S., Breard, C., and Diamond, J., "Demonstration of a CFD-CAA methodology to predict buzz-saw noise propagation to the aircraft," *AIAAP*, 2007.
- <sup>9</sup>Kurosaka, M., "A note on multiple pure tone noise," *J. Sound Vib.*, Vol. 19, No. 4, 1971, pp. 453–462.
- <sup>10</sup>Stratford, B. S. and Newby, D. R., "A new look at the generation of buzz-saw noise," *4th AIAA Aeroacoustics Conference, Atlanta, Georgia, USA, AIAA Paper 77-1343*, 1977.
- <sup>11</sup>Léwy, S. and Polacsek, C., "Analytical prediction of sound power radiated ahead of a transonic axial compressor or turbofan," *41st Inter-noise, New York City, USA*, 2012.
- <sup>12</sup>McAlpine, A., Schwaller, P., Fisher, M., and Tester, B., "Buzz-saw" noise: Prediction of the rotor-alone pressure field," *J. Sound Vib.*, Vol. 331, No. 22, 2012, pp. 4901–4918.





BP 72 - 29 avenue de la Division Leclerc - 92322 CHATILLON CEDEX - Tél. : +33 1 46 73 40 40 - Fax : +33 1 46 73 41 41

[www.onera.fr](http://www.onera.fr)